IV International Seminar on ORC Power Systems, ORC2017
13-15 September 2017, Milano, Italy

Experimental assessment of the open-source SU2 CFD suite for ORC applications

G.Gori[a], M.Zocca[a], G.Cammi[b], A.Spinelli[b], A.Guardone[a,*]

[a]Department of Aerospace Science & Technology, Politecnico di Milano, Via La Masa 35, 20156 Milano, Italy
[b]Energy Department, Politecnico di Milano, Via Lambruschini 4, 20156 Milano, Italy

Abstract

The first-ever experimental assessment of a Computational Fluid Dynamics (CFD) software for Non-Ideal Compressible-Fluid Dynamics (NICFD) flows of interest for ORC applications is presented here. Numerical results using SU2, the open-source suite for multi-physics simulation and design recently extended to deal with complex thermodynamic models of organic fluids, are compared here to experimental results from the Test-Rig for Organic VApours (TROVA) of the Laboratory of Compressible-fluid dynamics for Renewable Energy Applications (CREA), Politecnico di Milano. Experimental results regard supersonic expanding flows of siloxane fluid MDM (Octamethyltrisiloxane, $C_8H_{24}O_2Si_3$) in non-ideal conditions representative of ORC applications. Three different geometries are considered for the assessment of the CFD solver. The first is a converging-diverging nozzle, representative of ORC supersonic stators, in which the fluid is accelerated to supersonic speed from highly non-ideal conditions, with inlet compressibility factor $Z = Pv/(RT)$, computed using reference Equations Of State (EOS) for MDM fluid, as low as $Z \sim 0.81$. The second geometry is a diamond-shaped airfoil at a neutral angle of attack. The airfoil is plunged into a supersonic flow at Mach 1.5 and $Z \sim 0.9$, in mildly non-ideal conditions. Oblique shock waves are observed at the airfoil leading edge and interact with the wind-tunnel walls and the rarefaction fan from the airfoil. This test case is useful to understand the physics of oblique shock-wall and shock-shock interactions in turbine cascades operating in off-design conditions. The third geometry is a supersonic backward facing step, in which the formation of an oblique shock is observed experimentally at the reattachment point past the step. The Mach number is around 1.1 and the compressibility factor $Z \sim 0.89$. This geometry is representative of the trailing edge of turbine blades and it is useful to study the formation of fish-tail shock waves. These NICFD flows are fairly well captured by the CFD solver, thus confirming the validity of both the thermodynamic models and of the CFD implementation, using both the Euler equations for inviscid flows with negligible thermal conductivity and the full Reynolds-averaged compressible Navier-Stokes equations, for non-ideal compressible turbulent flows. In the considered shocked flows, grid adaptation is found to be key to capture the relevant flow features using a reasonable amount of grid points.

* Corresponding author.
E-mail address: alberto.guardone@polimi.it

1. Introduction

The design of turbine blades, and of diverse components of an Organic Rankine Cycle (ORC) power system, requires one to account for a possible non-ideal behaviour of the working fluid in the operating conditions of interest. Within the turbine vane, the molecularly complex organic fluid usually operates in thermodynamic conditions close to the liquid-vapour saturation curve and close to the critical point, thus resulting in high compressibility and low speed of sound. As a consequence, the fluid velocity often exceeds the speed of sound and supersonic flows are observed at the trailing edge. Such regime is commonly referred to as non-ideal since thermodynamic properties of the fluid can no longer be correctly described by means of the well-established equation of state (EoS) for ideal, dilute gases. The branch of fluid mechanics devoted to the study of these flows is termed Non-Ideal Compressible-Fluid Dynamics or NICFD.

The numerical simulation of flows of interest for ORC applications therefore calls for Computational Fluid Dynamics (CFD) softwares embedding highly accurate—but unfortunately complex and computationally expensive— non-ideal thermodynamic models. Currently, only a few CFD codes are capable of simulating flows in the non-ideal regime. Indeed, the vast majority of CFD solvers rely on the general assumption of that the fluid obeys the ideal gas law. From a numerical standpoint, the ideal gas assumption leads to a set of simplifications that are often exploited to optimize the performance of the software. Among many, the fact that the speed of sound and the specific internal energy and enthalpy are functions of the fluid temperature only greatly simplifies CFD algorithms. Remarkably, none of the currently available NICFD CFD codes was ever validated against measurements in the NICFD regime. The accuracy of results from simulations, which amplifies the *unknown* accuracy of the underlying thermodynamic models, is therefore highly questionable.

This paper presents the first-ever assessment of a NICFD flow solver against experimental data. Experimental results were collected using the Test-Rig for Organic VApours (TROVA) of Politecnico di Milano [1–3]. The TROVA was designed to investigate the expansion of molecularly complex fluids in the NICFD region of interest for ORC applications. The plant operates as a blow-down wind tunnel: the fluid is charged into a high pressure vessel where it is heated isochorically. As the control valve is opened, the fluid is expanded through a converging-diverging nozzle to be eventually recovered in a low pressure vessel. The test section is the converging-diverging nozzle, where pressure, temperature and velocity measurements are carried out independently, at selected locations. Thermocouples and pressures transducers have been calibrated using the exact measurement chain used during the experiment, following the guidelines reported in [4]. Calibration cycles have been performed, for every pressure transducers, at different temperatures. Calibration curves have been extrapolated together with the value of extended uncertainties related to each thermocouple and to each pressure transducer; the latter as a function of the temperature. The obtained values are representative of the overall measurement uncertainties. In practice, experimental error bars are not reported in plots presented hereinafter since they turned out to be remarkably small, if compared to the overall graph scale. Therefore it would be impossible to distinguish error bars in plots. Moreover, the TROVA is equipped with an optical schlieren apparatus [5,6]. Results presented in the present paper refer to non-ideal supersonic flows of siloxane fluid MDM (Octamethyltrisiloxane, $C_8H_{24}O_2Si_3$). The TROVA facility is designed to operate with both siloxane and perfluorocarbons that are of interest for ORC application. The facility is now being modified to deal with binary mixtures of siloxane fluids.

The NICFD CFD code considered here is the SU2 suite, an open-source platform designed to solve multi-physics Partial Differential Equation (PDE) problems and PDE-constrained optimization problems [7,8], which was recently extended to NICFD flows [9–11]. The SU2 NICFD solver is equipped with an embedded thermodynamic library which includes the ideal EoS, the van der Waals cubic EoS (VDW) and the improved Peng-Robinson Stryjek-Vera EoS (iPRSV) [12]. Moreover, a C++ interface to the multi-purpose thermodynamic library FluidProp [13,14], provides access to state-of-the-art fluid models, including multi-parameter EoS. The mesh adaptation procedure reported in [15] is applied. Mesh adaptation allows to improve the quality of unstructured two-dimensional hybrid meshes in regions characterized by large gradients such as, for instance, shock waves.

Three different geometries, including both two- and three-dimensional cases, are considered to assess the capability of the CFD solver in simulating flows of interest for ORC applications. A supersonic non-ideal expansion through a converging-diverging nozzle, representative of ORC supersonic stators, is studied in Sec. 2. Sec. 3 reports of the supersonic flow around a diamond-shaped airfoil to investigate shock-shock and shock-boundary layer interaction
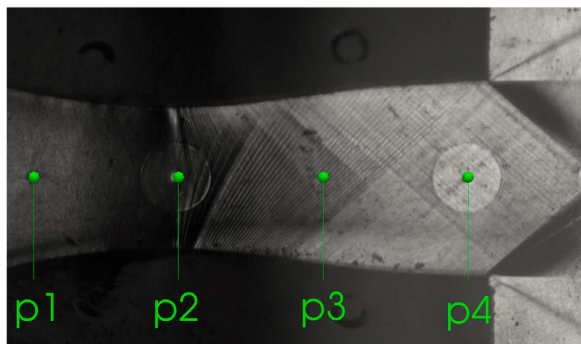
Fig. 1. Schlieren image of the under-expanded flow within the diverging section of the nozzle.

within the non-ideal regime. The third test case, presented in Sec. 4, regards the supersonic flow over a backward facing step that reproduces the shock wave pattern which is typically built at the trailing edge of a turbine blade of finite thickness. Eventually, Sec. 5 briefly summarizes the outcome of the paper.

2. Non-ideal supersonic expanding flow

An investigation of the non-ideal flow of MDM expanding in a converging-diverging nozzle is presented in this section. This geometry is representative of ORC supersonic stators, in which the fluid is accelerated to supersonic speed from highly non-ideal conditions. The compressibility factor at the inlet $Z = Pv/(RT)$, computed using the reference EoS for MDM fluid proposed in [16], is as low as $Z = 0.81$. Fig. 1 reports a schlieren image of the test section during the experimental run: the image is focused on the diverging section of the nozzle and the position of each pressure tap is highlighted using green dots along the nozzle axis. The schlieren image reveals an almost uniform flow within the nozzle: weak waves arise from small flaws along the upper and lower wall surface of the nozzle due to machining. Test conditions result in an under-expanded supersonic flow and hence two symmetrical rarefaction fans are clearly visible at the nozzle discharge section (dark triangular regions on the right hand side of Fig. 1). Pressure measurements are available along the symmetry axis of the nozzle, at selected location.

The computational domain considered for all CFD simulations is limited to the converging and the diverging sections of the nozzle. The conditions of the fluid at the inlet boundary reproduce the state measured experimentally within the settling chamber, right before the nozzle (total pressure and temperature correspond to 458569.3 [Pa] and 512.57 [K], respectively). No boundary condition is required at the exit section due to the supersonic character of the flow. Numerical results include steady simulations of inviscid and viscous flows, using diverse thermodynamic models, namely the ideal gas law, the iPRSV model and the reference fluid model based on the Helmholtz EoS [16] implemented in the FluidProp library. The value of the compressibility factor along the axis of the nozzle is reported in Fig. 2(a) respectively as computed from the ideal, the iPRSV and the reference EoS. The value of Z is significantly below unity throughout the whole centerline, suggesting that the flow can be indeed properly classified as non-ideal.

Numerical simulations were first carried out using different levels of grid resolution to evaluate the dependency of the solution on the spatial discretization, under the inviscid-flow assumption and by considering a two-dimensional domain. The grids are referred to as grid 1 (307 points), grid 2 (1 081 point), grid 3 (3 995 points) and grid 4 (15 310 points) in the following. Fig. 2(b) shows a comparison of pressure trends computed numerically along the nozzle centerline, for each grid, using the iPRSV EoS. No significant difference is observed among the curves reported in Fig. 2(b). This suggests that an adequate level of grid resolution was reached and that the solution does no longer depend on the spatial resolution of the grid. Fig. 3(a) depicts pressure profiles computed using the diverse EoS. The ideal model delivers a pressure distribution that qualitatively resembles the actual behavior of the fluid, but it loosely approaches the measured values. Numerical results fairly reproduce the actual measurements along the axis of the
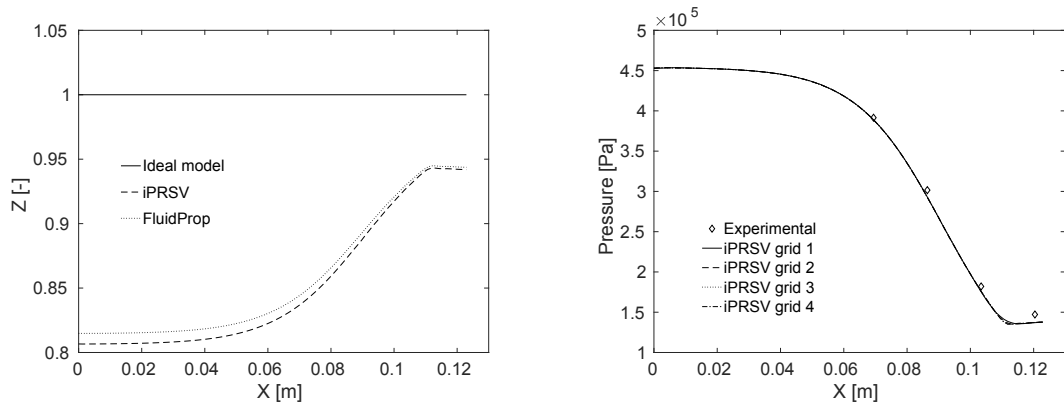
Fig. 2. (a) Compressibility factor along the nozzle axis resulting from SU2 NICFD simulations of an inviscid flow, using different EoS; (b) Comparison of pressure profiles along the axis of the nozzle from inviscid simulations over grids with different resolution
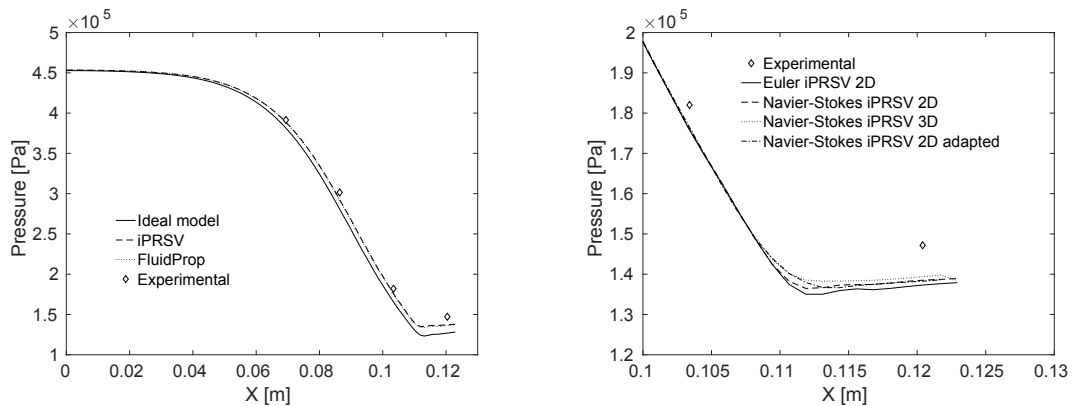

Fig. 3. (a) Comparison of pressure profiles along the nozzle axis for (a) different thermodynamic models and (b) viscous two- and three-dimensional simulations (enlargement at the nozzle exit).

nozzle. Small differences of about −7% are found only near the exhaust section, possibly due to boundary-layer effects that reduce the effective passage area. The iPRSV EoS and FluidProp produce similar results that better represent the measured pressure profile, thus confirming the need of including complex thermodynamic models in CFD simulations to represent NICFD flows properly.

To evaluate the validity of the boundary-layer approximation underlying the above inviscid-flow results, simulations based on the Reynolds-averaged Navier-Stokes equations were also carried out. For this test case, viscous simulations, including both two-dimensional and three-dimensional domains, take advantage of the turbulence model from Spalart-Allmaras [17] and the Menter Shear Stress Transport model [18]. No significant differences were found between the solution computed using the two turbulence model. Therefore, only the Spalart-Allmaras model is employed hereinafter. Fig. 3(b) reports an enlargement of the pressure profiles in the close proximity of the exhaust section, where larger differences are observed among numerical predictions. Results from viscous simulations are closer to the experimental ones, with particular reference to the terminal pressure plateau. This latter effect, possibly resulting from the reduction of the nozzle cross-sectional area due to the thickness of the boundary layer, is more relevant if a fully three-dimensional domain is considered because of the boundary layers along the the nozzle side-walls. The adaptive mesh procedure was applied to two-dimensional simulations to enhance the quality of the grid within the boundary layer. The grid adaptation did not yield to any remarkable improvement of the computed solution.
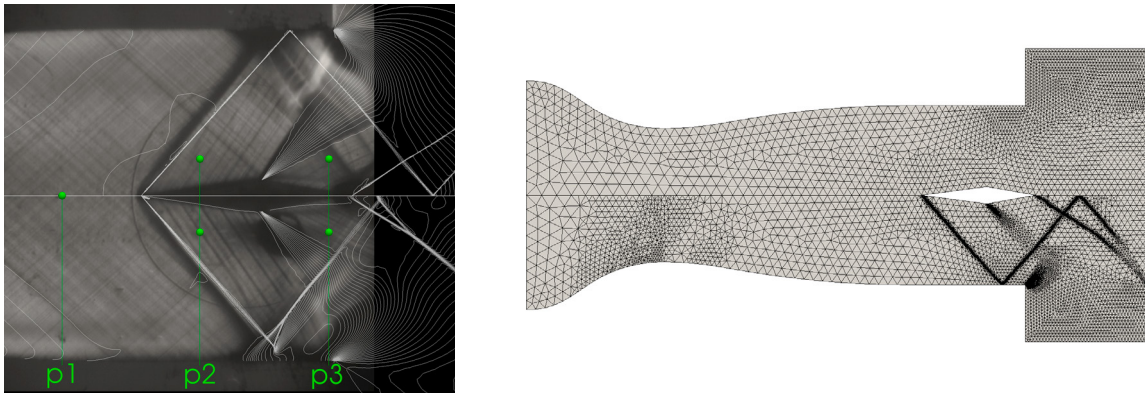
Fig. 4. (a) Experimental schlieren image of the supersonic flow field around the diamond-shaped airfoil. Density contours from inviscid (upper side) and from viscous (lower side) simulations, using the iPRSV EoS, are superimposed. Green dots indicate the position of pressure taps; (b) The upper half depicts the baseline numerical grid while the lower side reports the grid resulting after six steps of mesh adaptation procedure;

3. Non-ideal flow around a diamond-shaped airfoil

The second test case regards the non-ideal supersonic flow of MDM over a diamond-shaped airfoil at neutral angle of incidence. The test-rig is here used as a supersonic wind tunnel, fluid conditions within the settling chamber are $P^t = 870759.2$ Pa and $T^t = 550.77$ K. The nozzle is designed to produce a supersonic uniform flow at the exit section, where the airfoil is placed, see [1,2]. The airfoil is symmetrical with respect to his chord ($c = 36$ [mm]). The angle of the diamond at the leading and at the trailing edge is equal to 15 and 20 degrees, respectively. The channel around the airfoil is 56.4 [mm] wide. The terminal section of the divergent is visible in Fig. 4(a). Ahead of the airfoil, the flow is approximately uniform at Mach 1.5 and $Z = 0.9$, in mildly non-ideal conditions. Oblique shock waves are observed at the airfoil leading edge and interact with the wind-tunnel walls and with the rarefaction fans from the airfoil. This test case is useful to understand the physics of oblique shock-wall and shock-shock interactions in turbine cascades operating in off-design conditions.

Pressure measurements at discrete points and the schlieren image of a wide portion of the test section are thus available for comparison in Fig. 4(a). Static pressure is measured at the locations marked with green spots in Fig. 4(a). The first tap $p1$ is located along the nozzle axis, within the uniform flow region upstream of the nozzle exhaust section. The other pressure taps are arranged symmetrically on the upper and lower side of the airfoil. They are located in the uniform flow regions downstream of the shock waves $p2$ and of the expansion fans $p3$ originating on the airfoil. The schlieren image confirms the occurrence of shocks within the domain, as a consequence of the supersonic character of the flow. To accurately capture these discontinuities, the mesh adaptation procedure was heavily exploited. Fig. 4(b) depicts the numerical domain: the upper side reports the baseline grid while the lower side represents the numerical grid after six steps of adaptive refinement. The final grid counts almost 8 times the number of elements of the baseline mesh. With reference to Fig. 4(b), the grid is automatically refined to capture shocks and rarefaction fans with an appropriate level of resolution. Fig. 5(a) reports the pressure profiles, computed for different levels of mesh adaptation, obtained from inviscid simulations of MDM vapor modeled using the iPRSV EoS. Trends were extracted along a line parallel to the nozzle axis, at a distance of 6.25 mm from the centerline, which corresponds to a straight line through pressure taps $p2$ and $p3$. It has to be remarked that, differently from $p2$ and $p3$, the value of pressure $p1$ is measured along the nozzle axis but it is actually compared against its numerical value at a distance of y=6.25 mm: the flow before the diamond is uniform thus the pressure can be considered almost constant in a direction normal to the nozzle axis. Fig. 5(a) shows that the adaptive procedure allows to improve the resolution of the computed solution. Turbulent viscous simulations using the Spalart-Allmaras turbulent model [17] were also carried out. Fig. 5(b) reports a comparison of the pressure trends obtained from both inviscid and viscous simulations using both the iPRSV EoS and FluidProp, against the experimental measures at $p1$, $p2$ and $p3$. In Fig. 5(b) a highly non-ideal behavior is observed, the compressibility factor Z is approximately equal to 0.89 in the region of the flow before the diamond. In particular, the ideal pressure trend departs significantly from experimental measurements. On the other hand, numerical results
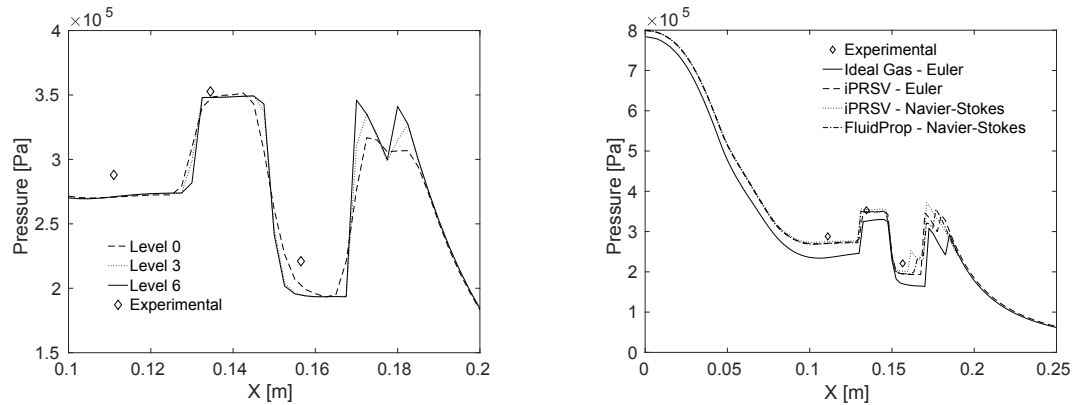
Fig. 5. (a) pressure trends from inviscid simulations for different adaptation steps are compared against the experimental result. Picture shows an enlargement focused on the region close to the diamond-shaped airfoil; (b) pressure trends from inviscid and viscous simulation using the iPRSV EoS are compared against the experimental measure. Pressure trend computed for an inviscid ideal flow is also compared;

that take advantage of the iPRSV EoS reproduce the experimental data correctly. Viscous effects cannot be properly evaluated since such analysis is limited to a small portion of the domain which is far from the boundary layer.

Density contours are plotted over the schlieren image corresponding to the conditions simulated here. Fig. 4(a) reports density contours of both inviscid and viscous simulation using the iPRSV EoS, respectively on the upper and on the lower side. Viscous effects are of utmost importance, as expected, in the close proximity of channel walls, where the boundary layer is thicker. Indeed, the schlieren image shows that, near the wall, the typical structure arising from the interaction of the leading shock-wave with the boundary layer occurs. The inviscid simulation is not able to capture this feature and that is the reason why, though the angle of the leading wave is predicted fairly well, the shock pattern in the downstream portion of the domain does not match the experimental one. Instead, density contours from Navier-Stokes simulations, on the lower side of Fig. 4(b), clearly reproduce the shock-boundary layer interaction phenomenon. The shock wave pattern predicted by viscous simulations thus resembles the observed pattern throughout the whole domain. In particular, the leading shock-wave is correctly reflected at the wall angle and matches almost perfectly its counterpart on the schlieren image. It is worth to point out that such comparison provides only qualitative information.

4. Backward facing step

The third geometry is a supersonic backward facing step, in which the formation of an oblique shock is observed experimentally at the reattachment point past the step. This geometry is representative of the trailing edge of turbine blades and it is useful to study the formation of fish-tail shock waves. A converging-diverging nozzle characterized by a profile similar to the one presented in Sec. 2 is placed in the test section of the TROVA test rig. The profile was wrought to obtain a backward facing step of height $h = 0.1$ [mm] at the throat section, which is 8.4 [mm] wide, on both sides of the nozzle [5,19,20]. Test conditions within the settling chamber are $P^t = 457746.8$ Pa and $T^t = 520.1$ K. The value of the compressibility factor Z in the settling chamber is equal to 0.82 then it increases monotonically up to 0.98 at pressure tap $p8$. At the nozzle throat section, the Mach number is around 1.1 and the compressibility factor $Z \sim 0.89$.

Fig. 6(a) reports a schlieren snapshot of the test section and the position of each pressure tap. The presence of a backward facing step results in a complex (symmetrical) system of shock-waves that are reflected against the nozzle wall further downstream. The mesh adaptation procedure was found to be key to improve the resolution of the computed flow-field and, at the same time, to limit the size of the computational grid. Density contours are reported in Fig. 6(b): picture shows an enlargement of the nozzle throat region and density contours are superimposed on the experimental schlieren image. Fig. 6(b) reports also, on the lower side, the computational grid resulting after 2 steps
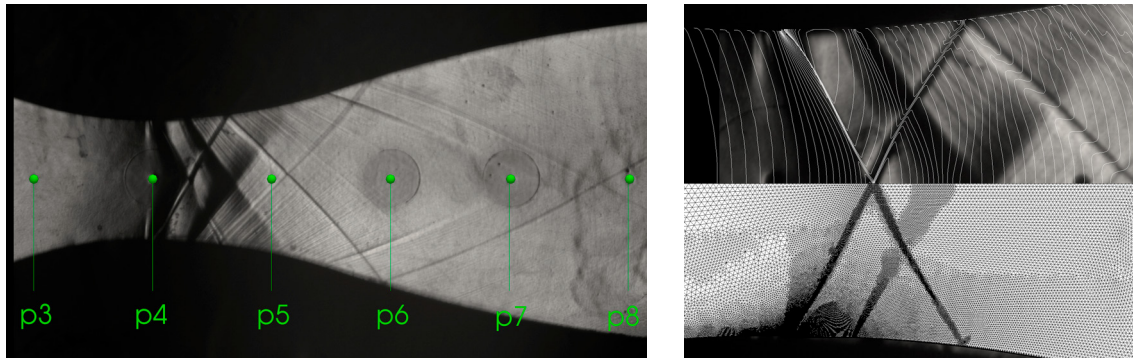
Fig. 6. (a) schlieren image of the flow-field within a nozzle with a backward facing step at the throat. Green dots indicate the position of pressure taps; (b) An enlargement of the nozzle throat section. On the upper side density contour from viscous simulation using the iPRSV EoS are superimposed to the schlieren image. On the lower side, the numerical grid after two steps of adaptation procedure is reported.
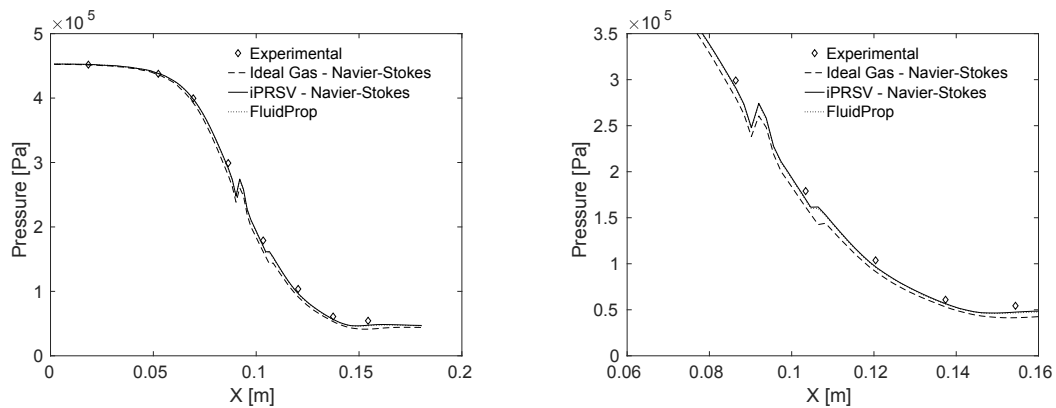

Fig. 7. (a) Comparison of pressure trends along the axis of the nozzle computed from viscous simulations for backward facing step test case; (b) Enlargement of the pressure trends along the axis of the nozzle computed from viscous simulations for backward facing step test case;

of adaptive refinement. The resolution of the grid is correctly increased in the close proximity of shock-waves and within rarefaction fans.

Fig. 7(a) reports pressure trends along the nozzle axis. The experimental measure is compared against the pressure trend computed using the ideal gas law, the iPRSV EoS and FluidProp. Both the iPRSV EoS and the fluid model from FluidProp are found to better represent the experimental measurements, thus confirming the occurrence of NICFD behaviour.

5. Conclusions

For the first time, the capabilities of a Non-Ideal Computational Fluid Dynamics (NICFD) solver were assessed against experimental results regarding flows of fluid in a non-ideal regime. Experimental data used for comparison were collected using the TROVA facility at Politecnico di Milano. The NICFD solver from the SU2 open-source suite was assessed for a set of exemplary NICFD flow-field that are relevant to ORC applications. These are the supersonic flow in converging-diverging nozzle, representative of ORC supersonic stators; a diamond-shaped airfoil at zero incidence in a supersonic flow, which is used to investigate the physics of oblique shock-wall and shock-shock interactions in turbine cascades; a supersonic backward facing step, in which the formation of an oblique shock is observed experimentally at the reattachment point past the step, resembling the formation of fish-tail shock waves at the trailing edge of turbine blades.

Numerical simulations are carried out using both the Euler equations for inviscid flows with negligible thermal conductivity and the full Reynolds-Averaged compressible Navier-Stokes equations for non-ideal compressible turbulent flows. In the considered shocked flows, grid adaptation is found to be key to capture the relevant flow features using a reasonable amount of grid points. All these NICFD flows are fairly well simulated by the CFD solver, thus confirming the validity of both the thermodynamic models and of the CFD implementation. The dilute, ideal gas model is found to fail in reproducing the experimental values, even in mildly non-ideal conditions. The need for the further development of NICFD solvers for ORC design is therefore confirmed.

Acknowledgements

References

[1] Spinelli, A., Pini, M., Dossena, V., Gaetani, P., Casella, F.. Design, simulation, and construction of a test rig for organic vapours. ASME J Eng Gas Turb Power 2013;135:042303.

[2] Guardone, A., Spinelli, A., Dossena, V.. Influence of molecular complexity on nozzle design for an organic vapor wind tunnel. ASME J Eng Gas Turb Power 2013;135:042307.

[3] Pini, M., Spinelli, A., Dossena, V., Gaetani, P., Casella, F.. Dynamic simulation of a test rig for organic vapours. In: Proceedings of 5th Conference on Energy Sustainability, ASME EsFuelCell2011, Washington, Washington DC, USA. 2011,.

[4] Joint Committee for Guides in Metrology, J.C.G.M.. Evaluation of measurement dataguide to the expression of uncertainty in measurement. Int Organ Stand Geneva ISBN 2008;50:134.

[5] Spinelli, A., Guardone, A., Cozzi, F., Carmine, M., Cheli, R., Zocca, M., et al. Experimental observation of non-ideal nozzle flow of siloxane vapor mdm. In: 3rd International Seminar on ORC Power Systems, Brussels, Belgium, 12-14 October. 2015,.

[6] Spinelli, A., Cozzi, F., Zocca, M., Gaetani, P., Dossena, V., Guardone, A.. Experimental investigation of a non-ideal expansion flow of siloxane vapor MDM. In: Proceedings of the ASME 2016 Turbo Expo, Soul. GT2016-57357; 2016,.

[7] Palacios, F., Colonno, M.R., Aranake, A.C., Campos, A., Copeland, S.R., Economon, T.D., et al. Stanford University Unstructured (SU^2): An open-source integrated computational environment for multi-physics simulation and design. AIAA Paper 2013-0287 2013;51st AIAA Aerospace Sciences Meeting and Exhibit.

[8] Economon, T.D., Mudigere, D., Bansal, G., Heinecke, A., Palacios, F., Park, J., et al. Performance optimizations for scalable implicit {RANS} calculations with {SU2}. Computers & Fluids 2016;129:146 – 158. URL: http://www.sciencedirect.com/science/article/pii/S0045793016300214. doi:http://dx.doi.org/10.1016/j.compfluid.2016.02.003.

[9] Vitale, S., Gori, G., Pini, M., Guardone, A., Economon, T.D., Palacios, F., et al. Extension of the su2 open source cfd code to the simulation of turbulent flows of fuids modelled with complex thermophysical laws. AIAA Paper 2015;2760:2015.

[10] Gori, G., Guardone, A., Vitale, S., Head, A., Pini, M., Colonna, P.. Non-ideal compressible-fluid dynamics simulation with su2: Numerical assessment of nozzle and blade flows for organic rankine cycle applications. In: 3rd International Seminar on ORC Power Systems. Brussels, Belgium; 2015,.

[11] Pini, M., Vitale, S.,,, Colonna, P., Gori, G., Guardone, A., et al. Su2: the open-source software for non-ideal compressible flows. In: NICFD 2016: 1st International Seminar on Non-Ideal Compressible-Fluid Dynamics for Propulsion & Power. Varenna, Italy; 2016,.

[12] Stryjek, R., Vera, J.H.. PRSV: An improved Peng-Robinson equation of state for pure compounds and mixtures. Can J Chem Eng 1986;64:323–333.

[13] Colonna, P., van der Stelt, T.P.. FluidProp: a program for the estimation of thermo physical properties of fluids. software; 2004. URL: http://www.fluidprop.com.

[14] Colonna, P., van der Stelt, T.. FluidProp: A program for the estimation of thermo-physical properties of fluids. Tech. Rep.; 2005. URL: http://dx.medra.org/10.2514/1.29718.

[15] Dussin, D., Fossati, M., Guardone, A., Vigevano, L.. Hybrid grid generation for two-dimensional high-reynolds flows. Computers & Fluids 2009;38(10):1863–1875.

[16] Thol M.and Herrig, S., Krber, M., Dubberke, F., Span, R., Vrabec, J.. Speed of sound measurements and a fundamental equation of state; 2016.

[17] Spalart, P., Allmaras, S.. A one-equation turbulence model for aerodynamic flows. AIAA Paper 1992-0439 1992;.

[18] Menter, F.. Zonal two equation $k - \omega$, turbulence models for aerodynamic flows. AIAA Paper 1993;93-2906.

[19] Cozzi, F., Spinelli, A., Carmine, M., Cheli, R., Zocca, M., Guardone, A.. Evidence of complex flow structures in a converging-diverging nozzle caused by a recessed step at the nozzle throat. In: J. Chem. Eng. 2016,.

[20] Spinelli, A., Cozzi, F., Cammi, G., Zocca, M., Gaetani, P., Dossena, V., et al. Preliminary characterization of an expanding flow of siloxane vapor mdm. In: 1st International Seminar on Non-Ideal Compressible-Fluid Dynamics for Propulsion & Power, Varenna, Italy, 20-21 October. 2016,.